Available online at www.sciencedirect.com
SCIENCE DIRECT®
Journal of Power Sources 122 (2003) 144–152
JOURNAL OF POWER SOURCES
www.elsevier.com/locate/jpowsour

Numerical simulation of porous networks in relation to battery electrodes and separators

Kamalnayan Kantilal Patel, Jens M. Paulsen, Johann Desilvestro*

Pacific Lithium (New Zealand) Limited, 2 Mana Place, Manukau City, New Zealand

Received 16 December 2002; accepted 14 February 2003

Abstract

Numerical simulation is used to explore the influence of particle shape and overall porosity on the liquid phase conductivity, σ_{eff}, inside porous networks, such as electrodes or separators used for lithium-ion batteries. Such battery components are often modelled by a power law, $\sigma_{\text{eff}} = \varepsilon^{\alpha}\sigma_0$, which relates electrolyte bulk conductivity σ_0 and void volume fraction ε via a Bruggeman exponent α. Frequently, a value of 1.5 is assumed for α. In this work, theoretical and experimental evidence is presented to show that a Bruggeman exponent of 1.5 is often not valid for real electrodes or separator materials. It is found that only idealized morphologies, based on spherical or slightly prolate (i.e. rod-type) ellipsoids, are expected to give rise to a Bruggeman law with an exponent of about 1.3. Porous networks based on other particle morphologies such as oblate (i.e. disk-type) ellipsoids or lamellar or flaky materials increase the tortuous path for ionic conductivity and result either in a significant increase of the exponent α, or in a complete deviation from the power law. These models imply that spherical or slightly prolate ellipsoidal particles should be preferred for batteries where high-rate performance is required and that future separators could be designed with higher ionic conductivity.

Keywords: Electrode modelling; Separators; Porous networks; Bruggeman law; MacMullin numbers; Lithium-ion battery

1. Introduction

Computers are becoming more and more powerful and more advanced software is constantly being developed. This makes it easier to simulate and thus understand and predict the performance of practical devices such as batteries, fuel cells or double-layer capacitors, by using models based on first principles. In this study, the focus is on general morphological characteristics of electrodes and separators used in lithium-ion batteries. The most significant early theoretical work on modelling battery systems, based on porous electrodes, was developed by Newman and Tobias in the 1960s and 1970s [1–3]. In more recent times, significant amount of modelling work on lithium-ion batteries has been presented [4–6]. A review of these publications show, however, that many parameters are not known experimentally. One major challenge is how to implement the morphology of real electrodes and separators. Usually, a quasi-continuous medium is employed, which simplifies the morphology of battery components towards a model described by a few parameters. Such parameters are normally only estimated. Therefore, numerical simulation of battery performance often requires model fitting and parameter adjustment.

One of the most important properties that limits the performance of lithium-ion batteries at high rates is the transport of lithium ions in the electrolyte. The overall transport of ionic charges across the cell occurs almost exclusively in the liquid electrolyte. Transport of lithium ions in the solid phase takes place mainly within single particles, where diffusion lengths are much shorter than the thickness of the whole electrode. Thus, open liquid porosity is required to achieve sufficient performance, particularly at higher rates of discharge. The relatively poor ionic conductivity of electrolyte solutions based on organic solvents limits the thickness of electrodes when reasonable discharge rates have to be obtained. Practically, the thickness of electrode layers in lithium-ion batteries is limited to a maximum of about 0.15–0.2 mm, because complex electrolyte transport phenomena, such as field-assisted migration and coupled diffusion of positive and negative ions, cause electrolyte depletion and accumulation at the higher rates, which further decreases the electrolyte conductivity. Design of practical battery electrodes is always a compromise between minimum electrode thickness for maximum specific power and maximum thickness for higher specific energy and lower cost. Because of the importance of electrode and separator

* Corresponding author. Tel.: +64-9-261-1365; fax: +64-9-263-4137.
E-mail address: hans@pacificlithium.co.nz (J. Desilvestro).

0378-7753/03/$ – see front matter © 2003 Elsevier Science B.V. All rights reserved.
doi:10.1016/S0378-7753(03)00399-9

morphology for battery design, this study examines the ionic conductivity in the liquid phase inside porous structures.

Practical battery electrodes normally consist of a composite of active-material powder, polymeric binder, and electronically conductive additives such as carbon. Each of the components may have its distinctive distribution of particle sizes and shapes. Thus, a porous network of interconnected pores is formed, and the pores are then filled with liquid electrolyte. This structure is very complex. A complete description would require an intricate model with a large number of parameters. Simulations are only practically possible if the structure is represented by a simplified quasi-continuum involving a few parameters. In such an approach, the 'effective' electrolytic conductivity, σ_{eff}, is often defined by [2,7]

$$\sigma_{\text{eff}} = \varepsilon^{\alpha}\sigma_0, \quad \alpha \cong 1.5 \tag{1}$$

where σ_0 is the bulk ionic conductivity of the electrolyte, ε is the void volume fraction of the porous electrode or separator filled with electrolyte, α is the Bruggeman exponent. The validity of this relation has been shown [7] for the electrolytic conductivity in a variety of porous beds of spherical particle, and was even approximated for samples of sandstone with void volume fractions down to 0.1 when the exponent α is adjusted to 1.6–1.7. Note that, a porosity of 10% is well below the closet-packing ($\varepsilon = 0.26$ for hexagonally, closest-packed spheres) and results from partial sintering or cementation. De La Rue and Tobias [8] performed careful experiments with glass beads of various sizes, suspended in saturated $ZnBr_2$ solutions, for relatively high void volume fractions of 1–0.6. It was found that suspensions based on monodisperse spherical particles were described rather well by a power law with α in the range 1.4–1.5. A similar relationship was observed even for beads with a size distribution between 50 and 6400 μm in diameter [8].

Nevertheless, the general applicability of $\alpha \cong 1.5$, appears questionable because particles used for battery electrodes are frequently not of an ideal shape. Graphite or metal oxide particles may in fact be flaky or irregularly-shaped ellipsoidal particles. Electrodes are usually compacted by a calendering step, where an alignment of particles may occur and result in film anisotropy. Electrodes in commercial cells may be calendered to porosity values below 0.26, i.e. beyond the limit of cubic or hexagonally closest-packed, uniform spheres, since polymeric binder and carbon can be squeezed into voids and because particles which consist of a distribution of sizes can pack tighter. In the work reported here, an investigation is made of the filling of interstices with smaller particles, which to our knowledge has not been explored theoretically before. While some authors assumed the validity of Eq. (1) with $\alpha = 1.5$ for simulating battery electrodes [4,9,10] or separators, Fan and White [11] chose an α-value of 2.5 for both electrodes and separators in Ni–Cd batteries. Doyle et al. [5] determined α-values of 3.3, i.e. significantly higher than 1.5, by fitting experimental discharge curves of $LiMn_2O_4$-based lithium-ion batteries. The same authors used an even higher Bruggeman exponent of 4.5 for quantifying the ionic conductivity of their plasticized electrolyte membrane [5]. Experimental data for separators, some from literature [12] and some from this work (v.i.), are only compatible with Eq. (1) if the formal Bruggeman exponent is adjusted to values significantly higher than 1.5.

Due to the lack of generally-accepted procedures to quantify electrolytic conductivity in practical porous battery electrodes, it is of interest to examine the validity of Eq. (1) for different morphologies by using computer simulations. This paper is organized in the following way. After an outline of the theoretical background, the experimental conductivity data for a variety of separator materials are presented and assessed in terms of Eq. (1). Numerical simulation results for electrodes based on spherical particles of uniform size are then discussed and the results compared with Eq. (1). Conductivity for configurations beyond the level of closest packing of uniform spheres is explored by placing smaller spherical particles into interstices between the larger ones. Then, consideration is given to configurations which are based on closely-packed spheres modified by introducing an anisotropy parameter which results in a formal deformation of spheres to aligned ellipsoids, while maintaining the overall porosity at a constant value. Finally, electrodes based on aligned, rather flat particles are explored by approximating them by a network of tiles. For each of the model cases, the dependency of conductivity on volume void fraction and film morphology are investigated in order to determine whether (1) can be applied. Conclusions are drawn on the relevance of this work to the design of battery electrodes and separators.

2. Theoretical

2.1. Bruggeman exponent and MacMullin number

The porosity ε of separators and electrodes can be measured directly (for example, by mercury porosimetry or pycnometry). The so-called MacMullin number N_{M} relates σ_{eff}, the effective electrolytic conductivity of a porous network, and σ_0, the ionic conductivity of the bulk electrolyte according to:

$$N_{\text{M}} = \frac{\sigma_0}{\sigma_{\text{eff}}} \tag{2}$$

Comparing Eqs. (1) and (2) yields:

$$N_{\text{M}} = \varepsilon^{-\alpha} \tag{3}$$

There is evidence that the power law, Eq. (1), with $\alpha = 1.5$ is not valid for real battery separators [12] (v.i.) and electrodes [5]. In principle, it would be more correct to avoid Eq. (1) and instead measure the MacMullin number and employ Eq. (2) for simulation of battery performance. This can be done in a straightforward way for separator membranes (see Section 3 below), but is more tedious for electrode films.

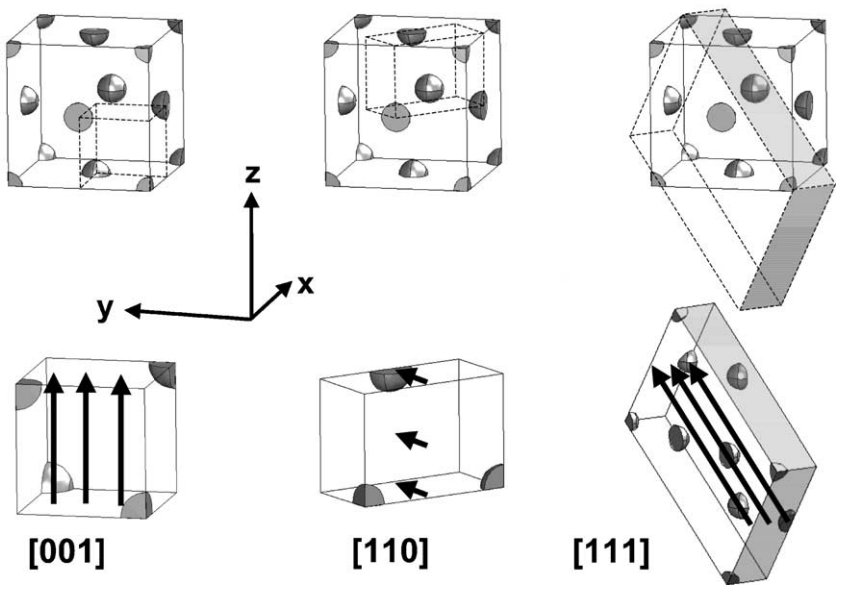

Fig. 1. Model geometries for calculating electrolytic conductivity of voids formed between monodisperse spheres in a fcc lattice. Representations in top line show 'conductivity unit cells' (dashed lines) used for calculating conductivity in the directions [0 0 1], [1 1 0] and [1 1 1], with respect to the fcc unit cell. Representations in bottom line detail conductivity unit cells with arrows that indicate the direction of current flow.

Abraham [12] suggested another relationship between the MacMullin number and porosity by introducing a tortuosity parameter, T, i.e.

$$N_{\mathrm{M}} = \frac{T^2}{\varepsilon} \tag{4}$$

By combining Eqs. (3) and (4), it is easy to transform T values [12] to formal Bruggeman exponents according to:

$$\alpha = 1 - \frac{2\log(T)}{\log(\varepsilon)} \tag{5}$$

2.2. Simulation of MacMullin numbers

If all relaxation and polarization effects can be neglected, the electrolyte conductivity, σ_0, is governed by Ohm's law:

$$\vec{j} = \sigma_0 \vec{E} \tag{6}$$

where j is the current density and E is the electrical field. If the conductivity is normalized to $\sigma_0 = 1$, the electrical field is defined as the gradient of the electrical potential, φ, by

$$\vec{E} = -\frac{\partial}{\partial \vec{r}}\varphi \tag{7}$$

Local charge neutrality requires

$$\frac{\partial}{\partial \vec{r}}\vec{j} = 0 \tag{8}$$

Assuming a constant conductivity in the electrolyte and inserting Eq. (6) into Eq. (8) yields the Laplace equation:

$$-\nabla^2\varphi = 0 \tag{9}$$

This equation is solved in the conductive volume with suitable boundary conditions for φ, and the normal derivative $\partial_n\varphi$. 'Conductivity unit cells' were defined by reducing the electrode morphology to the smallest possible cubic or rectangular prismatic unit, which is filled with the conductive medium (electrolyte) and excludes non-conductive regions which represent the particles. By way of example, Fig. 1 (left) shows how the electrolytic conduction in the [0 0 1] direction in a medium based on spherical particles stacked in a face-centred cubic (fcc) lattice was simulated in the void space of 1/8 of a fcc unit cell. The corresponding volume has a base ($z = 0$) and a top ($z = 1/2$). Boundary conditions are a fixed potential φ_1 at the base and a fixed potential φ_2 at the top; and the normal derivatives of the potential are zero at the four planes parallel to the current direction. 'Conductivity unit cells' used for conductivity simulation in the [0 0 1], [1 1 0] and [1 1 1] directions in a face-centred cubic lattice are shown in Fig. 1. For the [0 0 1] and [1 1 0] unit cells, the planes parallel to the current direction are mirror planes. Thus, there is no net current flow in or out of these planes and the boundary condition $\partial_n\varphi = 0$ is fulfilled. For the [1 1 1]-direction, the lightly shaded top plane in Fig. 1 and the corresponding bottom plane are not mirror planes. Nevertheless, the boundary condition was approximated by $\partial_n\varphi = 0$ at these two planes (see results and further discussion below).

The effective conductivity, σ_{eff}, and thus the corresponding MacMullin number, can be calculated from the current divided by the potential difference $\varphi_2 - \varphi_1$ between top and base. The current is obtained by integrating $\partial_n\varphi$ over the base surface or top surface; the index n indicates the current direction normal to the base or top surface. Alternatively, the current can be obtained by integrating $\partial_n\varphi$ over the volume and dividing by the distance between top and base. A

gradual increase of the radius of the spheres delivers the effective conductivities and MacMullin numbers as a function of porosity.

The calculations were made using the program package FEMLAB, running in conjunction with MATLAB on a standard PC. FEMLAB is a program package for solving partial differential equations. The Laplace equation (Eq. (9)) was solved using a mesh with about 20,000 nodes and elements. The mesh was automatically adapted to suit the given geometry. The accuracy was checked by using mesh refinement. Standard FEMLAB routines were used to perform the surface integration for $\partial_n\varphi$ and the volume integration for $\partial_z\varphi$. In the vicinity of closest packing, i.e. when the conductive channels became very narrow, numerical convergence problems occurred. Those results were discarded.

3. Experimental

A number of microporous polyolefinic separator membranes were saturated with an electrolyte solution of 1 M $LiPF_6$ in a 1:1 (wt:wt) mixture of ethylene carbonate and diethyl carbonate, and their conductivity was measured by two-point ac impedance. For each separator material, a circular piece of electrolyte-saturated membrane of 16 mm diameter was placed inside a 2032 button cell between two stainless-steel discs of 16-mm diameter and 1-mm thickness. A spring load was placed between one of the stainless-steel disks and the cell can. Cell cans, lids, grommets and spring loads were obtained from Hohsen Corporation. Cells were assembled in an argon-filled glovebox. The porosity and thickness of the separator samples are based on values provided by the manufacturers. The resistance of each sample was determined from the resistive part of the complex impedance at 60 kHz. The results were corrected for the combined electrical contact resistance of lid-to-steel disc, steel disc-to-spring load, and spring load-to-cell can. This overall contact resistance was determined to be 0.35 Ω. From the corrected resistance and thickness of each separator sample, the effective conductivity was obtained. The conductivity of the bulk electrolyte was measured by ac impedance at the same ambient temperature, using a standard conductivity cell, and the MacMullin number was obtained from Eq. (2). No correction was made for possible partial compression of separator membranes inside a real battery.

4. Results and discussion

4.1. Conductivity measurements with various separators

The porosity values as given by the manufacturers, measured MacMullin numbers and formal Bruggeman exponents derived using Eq. (3) are listed in Table 1 for a variety of commercially available separator materials. With the exception of one product with a very high porosity of 85%, most membranes yield formal Bruggeman exponents of 3–4. The Bruggeman exponents of all tested separator materials are significantly higher than 1.5. The results from this work are qualitatively in agreement with tortuosity data reported by Abraham [12] for 21 separator samples. Formal Bruggeman exponents can be calculated from Abraham's data using Eq. (5). Apart from one α-value of 0.4, they vary between 1.5 and 6.6, with the majority being between 2.3 and 4.4. Note that, a value below 1 is physically impossible. Theoretically, a Bruggeman exponent of 1 could be obtained if a separator consists of a material with straight, parallel channels, which are all perpendicular to the separator surface. The porosity values for the same product designation may vary to a certain degree. As an example, Celgard 2400 is specified by a 'typical' porosity value of 37%, while the manufacturer's product documentation lists values varying between at least 35 and 41%. For the same product, Abraham [12] used a porosity of 32%. An uncertainty in porosity between 35 and 41% for this product results in a range of Bruggeman exponents of between 2.63 and 3.09.

Table 1
Porosity values, ε, provided by manufacturer, MacMullin number, N_M, obtained from conductivity measurements and Bruggeman exponents, α, derived using Eq. (3) for various commercial microporous separators

Separator sample	ε	N_M	α
Celgard 2400	0.37	15.7	2.8
Celgard 2500	0.55	8.5	3.6
Solupor 14P01A	0.45	22.1	4.0
Solupor 7P03A	0.85	4.3	10.4
Hipore N962C	0.45	16.1	3.7
Hipore N720	0.37	19.3	3.1
Hipore 6022	0.50	13.4	3.9
Teklon 'Li-ion', 25 μm	0.45	12.9	3.4

Because of the very different processes used for separator and electrode manufacture, separators generally have a very different morphology from composite electrodes based on inorganic materials. Practically, the porosity of microporous membrane separators is often created by stretching the membrane and thus creating an array of pores of particular shape and size that depends on the process conditions. A separator has to fulfill a variety of functions, namely; to insulate anode and cathode from each other, provide a maximum of ion transport, and assure sufficient wettability. In addition, often a shut-down function is desired for product safety. Contrary to lithium-ion batteries in which a low tortuosity is desired, in lithium metal-based batteries a tortuous path in combination with a uniform current distribution over the whole electrode/separator interface, is sought in order to minimize dendrite growth, which may propagate from points of increased current density. Because of all these requirements, it is not straightforward to state from first principles what separator morphology is 'best'. Purely for maximizing high-rate performance, the overall separator/electrolyte resistance has to be minimized. With a given electrolyte system, this can be achieved by minimizing separator thickness and N_M. Thus,

separators with a high porosity, a low Bruggeman exponent and minimum thickness are desirable solely from the power performance point of view.

Since it is experimentally easy to determine the main parameter which governs the behaviour of the electrolytic quasi-continuum of the porous network inside a separator, i.e. the MacMullin number, there is not an immediate incentive to model separator structures. In principle, a similar approach to that used for characterizing the electrolytic transport properties by ac impedance could be applied to battery electrodes. The results would be of significant practical interest. The experiment is, however, not as straightforward as for separator materials since it is difficult to obtain free-standing films of electrodes (without substrate), which have the same composition and morphology as industrial electrodes. Additionally, the measurement of the ionic conductivity of the films would require the use of at least one additional separator layer to suppress the electronic conduction between the blocking electrodes (e.g. stainless-steel) and the porous electrode to be characterized. The main scope of the present study is to explore theoretically a broad range of configurations that model idealized morphologies of battery electrodes, rather than to develop an experimental technique or to characterize specific electrodes.

4.2. Simulation of various electrode morphologies

4.2.1. Spherical particles

First, it was investigated whether numerical simulation reproduces the experimentally observed power law with a Bruggeman exponent $\alpha \cong 1.5$ [7,8] for conductive liquids inside a bed of uniform spherical particles. The effective conductivity is shown in Fig. 2 as a function of the volume fraction filled with the conductive liquid. The volume fraction was varied by gradually increasing the radius of the spheres on their respective lattice positions. The data were calculated by a series of simulations using the 'conductivity unit cell' shown in Fig. 1. The particle arrangement is based on face- or body-centred cubic unit cells (fcc or bcc). The simulations were made for different configurations and different current directions. Since the four side walls of the 'conductivity unit cells', i.e. those parallel to the current direction, are mirror planes for the [0 0 1] and the [1 1 0] direction, the use of the smallest unit cell is justified. As pointed out above, this is not the case for the 'conductivity unit cell' for the [1 1 1] direction, where the top plane (shaded lightly in Fig. 1) and the corresponding bottom plane are not mirror planes. Calculations were performed with 1 [1 1 1] 'conductivity unit cell' and with 5 such cells stacked on top of each other, i.e. stacked in the direction $[\bar{1}\,\bar{1}\,2]$, which is perpendicular to the plane shaded lightly. With the larger number of cells, the error from incorrect boundary conditions can be reduced.

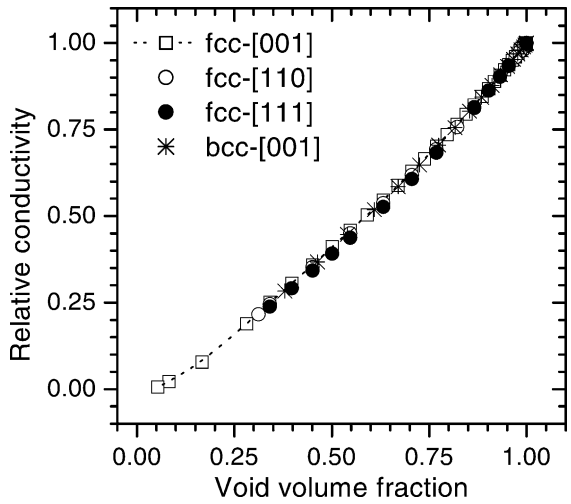

Fig. 2. Relative electrolytic conductivity of voids formed between monodisperse spheres in different directions in a fcc or a bcc lattice.

As seen in Fig. 2, the effective conductivity as a function of volume fraction from 100% void volume down to closest packing does not depend significantly on either the nature of the lattice (fcc or bcc) or the direction of the current chosen, at least for the investigated directions of [0 0 1], [1 1 0] and [1 1 1] for fcc. A smooth dependence of σ_{eff} on porosity is obtained in this region. For a fcc lattice, a 28% void volume fraction is near to the situation of closest-packed spheres ($\varepsilon = 0.26$). For a bcc lattice, closest packing corresponds to a 32% void volume fraction. A power law is valid and a fit for the Bruggeman exponent α shows that the following relation holds:

$$\sigma_{\text{eff}} = \varepsilon^{\alpha}\sigma_0 \text{ or } N_{\text{M}} = \varepsilon^{-\alpha}, \quad \alpha \cong 1.3 \tag{10}$$

The Bruggeman exponents for the various geometries which were simulated in this work are summarized in Table 2. This analysis shows that the electrolytic conductivity is almost the same for 1 [1 1 1] 'conductivity unit cell' and for 5 stacked cells, which indicates that forcing the current lines parallel to the plane shaded lightly in Fig. 1 (due to the boundary conditions outlined above in Section 2.2) does not have a significant impact on the overall conductivity.

Smaller volume fractions were simulated by letting the spheres overlap, thus simulating a sintering process. The data in Fig. 3 show that below the level of closest packing, conductivity no longer follows the same exponential law, i.e. the dashed curve is not a straight line in the double

Table 2
Bruggeman exponents for electrolytic conductivity of voids formed between monodisperse spheres in different directions in a fcc or a bcc lattice

Lattice-[direction]	Bruggeman exponent
fcc-[0 0 1]	1.32
fcc-[1 1 0]	1.32
fcc-[1 1 1], 1 conductivity unit cell[a]	1.35
fcc-[1 1 1], 5 conductivity unit cells[a]	1.33
bcc-[0 0 1]	1.31

[a] See text.

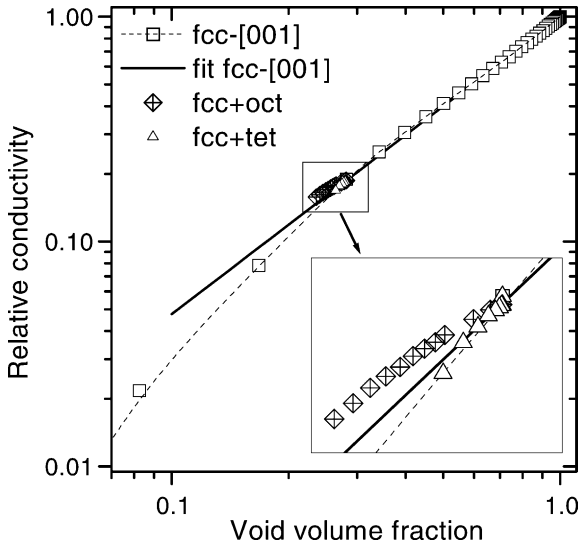

Fig. 3. Relative electrolytic conductivity of voids formed between monodisperse spheres in [1 1 0] direction of a fcc lattice, along with a fit according to Eq. (3). In addition, either octahedral or tetrahedral sites are filled with increasingly larger spheres (see text), thus further reducing void volume fraction.

logarithmic plot. Electrodes for commercial Li-ion batteries are generally not sintered. They normally consist, however, of a variety of particle sizes, which allows lower porosity values than found with monodisperse particles. This case was modelled by adding smaller spherical particles to an arrangement of spheres with a radius of 0.35 on the fcc sites. The radius $r = 0.35$ is a value just below $\sqrt{2}/4$ for closest packing. Octahedral sites (at each of the four free corners of the 'conductivity unit cell' in Fig. 1) or tetrahedral sites (in the centre of the 'conductivity unit cell') were filled. The radii of the smaller spheres were varied between 0 and <0.15 for the octahedral sites and from 0 to <0.08 for tetrahedral ones, i.e. just to a size where the smaller spheres almost contacted the larger ones. The insert of Fig. 3 shows that the conductivity slightly deviates from Eq. (10) for lower fractions of conductive volume, which is achieved by filling octahedral or tetrahedral sites.

In summary, simulations have reproduced the experimental result that a power law (Eq. (10)) is valid from 100% down to void volume fraction that correspond to closest packing. The exponent is slightly smaller than that experimentally determined for porous beds [7,8]. This may be due to the idealized packing arrangement in highly symmetric lattices, which does not fully reflect the situation in real packed or fluidized beds.

4.2.2. Ellipsoidal particles

Battery electrodes are normally very different from packed uniform spheres. Scanning electron micrographs of electrodes prepared on commercial coating equipment are shown in Fig. 4. The cross-section of an anode made from natural graphite (Fig. 4(A)) clearly shows that sheets or flakes of active material are partially aligned, leading to an anisotropic morphology. Obviously, the liquid diffusion paths across the electrode are quite long and the tortuosity for conduction across the pores of the electrode is large. A cross-section of a cathode which comprises transition metal oxide particles is shown in Fig. 4(B). Although the anisotropy is less pronounced, it is obvious that the particles are non-spherical and quite non-uniform.

Numerical computer simulations of configurations were undertaken when a change was made from an isotropic morphology to an anisotropic one, while maintaining porosity constant. Starting from the fcc configuration shown in Fig. 1, the unit cell and the spheres were elastically deformed by formally 'compressing' in the z-direction (=current direction). Thus, the spheres become oblate (disk-type) ellipsoids, aligned parallel to the electrode surface, and the cubic unit cell becomes a rectangular prism. In this case, the anisotropy parameter, R, is the ratio of the lengths of one of the two longer edges of the unit cell to the short edge (in z-direction),

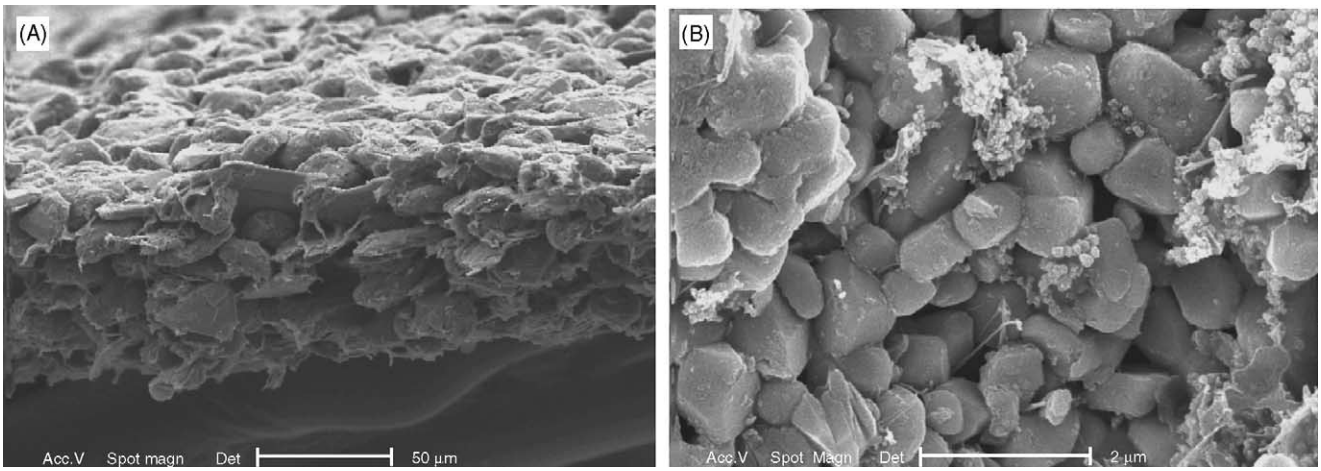

Fig. 4. Scanning electron micrographs of cross-sections of battery electrodes: (A) anode based on natural graphite; (B) cathode based on transition metal oxide material.

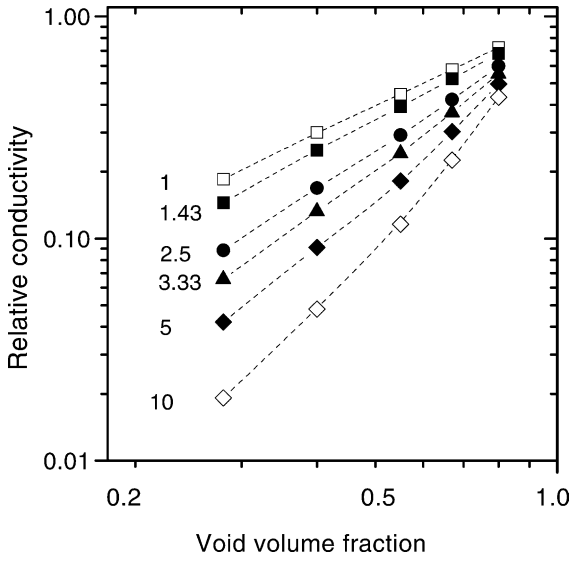

Fig. 5. Relative electrolytic conductivity of voids formed between monodisperse spheres ($R = 1$) or oblate ellipsoids in a fcc lattice as a function of porosity for an anisotropy parameter between $R = 1$ and $R = 10$.

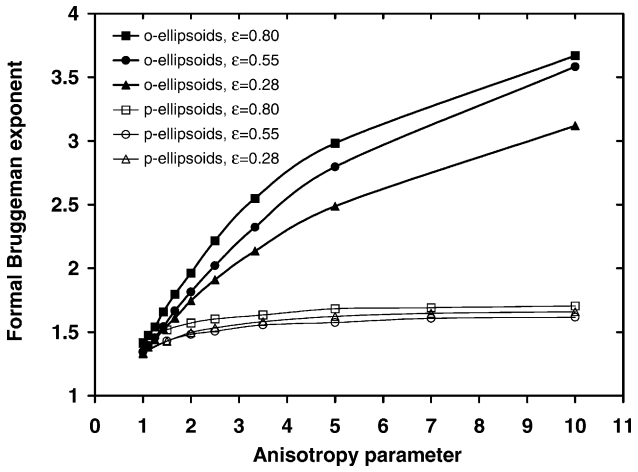

Fig. 6. Bruggeman exponents calculated for dispersions of oblate and prolate ellipsoidal particles in a fcc lattice as a function of lattice anisotropy for various porosity values. Anisotropy of parameter is defined as ratio of longer to shorter ellipsoid axes and is unity for spherical particles.

as well as the ratio of the long (x, y) to the short (z-direction) ellipsoid axes. Void volume fraction was varied by adjusting the volume of the ellipsoidal particles on their respective lattice positions, while maintaining their aspect ratio. The electrolytic conductivity is shown in Fig. 5 as a function of void volume fraction in a double logarithmic plot for various anisotropy parameters. With increasing anisotropy, the deviation from the strict power law (Eq. (3)) becomes more and more obvious. For practically important porosity values of 30–50%, however, still reasonably straight lines are obtained, as shown in Fig. 5. The slope and thus the formal Bruggemann exponents, calculated from data represented in Fig. 5 by applying Eq. (3) for each data point, increase with increasing anisotropy. The closed symbols in Fig. 6 are for oblate ellipsoids, the data show α-values of 1.3–2 for low anisotropy of $R < 2$. The Bruggeman exponent, however, increases quite rapidly with higher anisotropy, and results in significantly lowered conductivity values, especially for practically important porosity values of around 30%.

This analysis shows that a power law (Eq. (3)) approximates conductivity of an electrode based on disc-shaped spheroids of an anisotropy parameter (aspect ratio) up to 10 rather well, i.e. within approximately ± 0.1 α-units for practically relevant porosity values, when Bruggeman exponents significantly higher than 1.5 are employed.

Model calculations were also performed for prolate ellipsoids, i.e. by formally stretching the unit cell shown in Fig. 1 in the x-direction, resulting in rod-type ellipsoidal particles aligned in the x-direction, while maintaining the current in the z-direction. The curves with the open symbols in Fig. 6 show that the formal Bruggeman exponent for arrangements of prolate ellipsoids increases with increasing anisotropy from 1.3 to 1.6–1.7 and depends much less on the anisotropy parameter than for oblate ellipsoids. This result is also evident from a qualitative point of view, since the current lines basically encounter in the z-direction 'obstacles' with circular cross-sections in the case of prolate ellipsoids and 'obstacles' with elliptical cross-sections in the case of oblate ellipsoids, with a corresponding increase in tortuosity in the latter case.

In summary, α can be considered, in combination with Eq. (3), as a useful parameter for characterizing the quasi-continuum of a porous network based on spherical or ellipsoidal particles. The application of a power law is more justified than a tortuosity parameter according to Eq. (4) since simulated MacMullin numbers for electrode morphologies discussed up to now cannot be reasonably fitted by a $1/\varepsilon$ law. Nevertheless, caution is required to avoid oversimplification based on the presented simulations. The morphology of electrodes, especially as a result of coating and calendering, is certainly much more complex and results in an anisotropic compaction and partial alignment of non-spherical particles. Therefore, the conclusions of our calculations can only provide guidelines.

4.2.3. Rectangular prismatic particles

A set of model configurations was simulated to gain a better understanding of electrodes based on platelets or flakes, e.g. based on graphite (see Fig. 4(A)). In contrast to spherical and ellipsoidal particles, rectangular prismatic ones can be packed much tighter, in fact in the case of uniform size and shape to a theoretically zero void volume fraction. As for spherical particles, a model geometry has to be assumed, i.e. one that makes a compromise between random arrangement of particles in a real electrode and minimization of the size of the unit cell to be simulated. In practice, most platelet-shaped particles will be in a staggered orientation with respect to each other, but some may lie on top of each

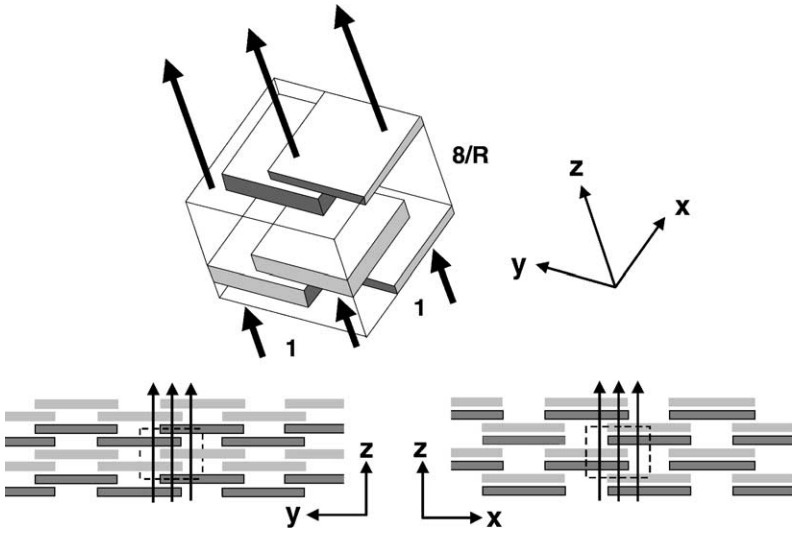

Fig. 7. Model geometry for calculating electrolytic conductivity of voids formed between square tile-shaped (or cubic) particles in a tetragonal (or cubic) lattice. Top: 'conductivity unit cell' with current flow in *z*-direction. Bottom: front and side views with conductivity unit cell (dashed lines).

other, at least when viewed from a particular direction. This situation is reflected by the simplified unit cell arrangement presented in Fig. 7 with sides 1, 1 and 8/*R*, where the anisotropy parameter *R* is unity for cubic particles. In this model configuration, the tiles are perfectly staggered when viewed in the *x*-direction (Fig. 7, bottom left), while 50% of them face each other over a much larger fraction of their surface, which is apparent when viewed in the *y*-direction (Fig. 7, bottom right). As with ellipsoids, the conductivity was calculated as a function of anisotropy by formally compressing the 'conductivity unit cell' shown in Fig. 7 and the prismatic particles in the *z*-direction. With increasing formal compression, flatter and flatter square tiles are obtained with a ratio *R* between the length (*x*-, *y*-directions) and the height (*z*-direction) of the tiles. Porosity was varied by formally increasing or decreasing the size of the prismatic particles on their respective lattice positions. As seen in Fig. 8, there is a large difference in formal Bruggeman exponents for different porosity values, which shows that a power law (Eq. (3)) is no longer applicable. The results were therefore tested to determine if Eq. (4) would represent a better description of electrolytic conductivity in such arrangements. Almost perfect straight lines are shown in Fig. 9, with slopes, *s*, which all intersect at $N_M \cong 1$ for $1/\varepsilon = 1$ (i.e. for the bulk electrolyte) and are described by

$$N_M = s\left(\frac{1}{\varepsilon} - 1\right) + 1 \tag{11}$$

For anisotropy values of $R \geq 2.5$, the slopes of the lines approximate *R* to within better than ±10%. Thus, Eq. (11) can be rewritten as

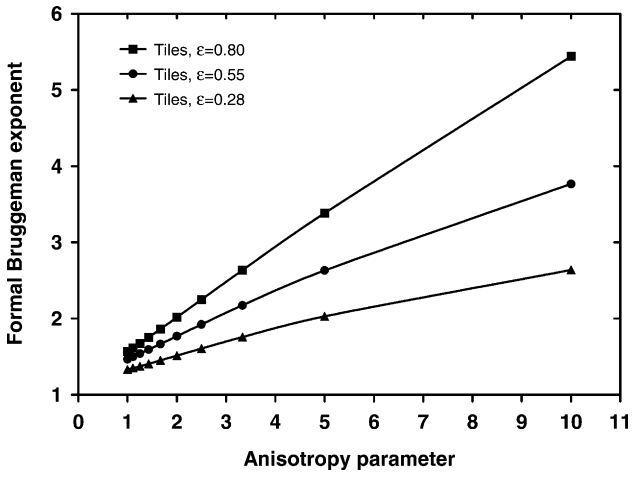

Fig. 8. Bruggeman exponents calculated for cubic or rectangular-prismatic particles, dispersed according to Fig. 7, as function of lattice anisotropy for various porosity values.

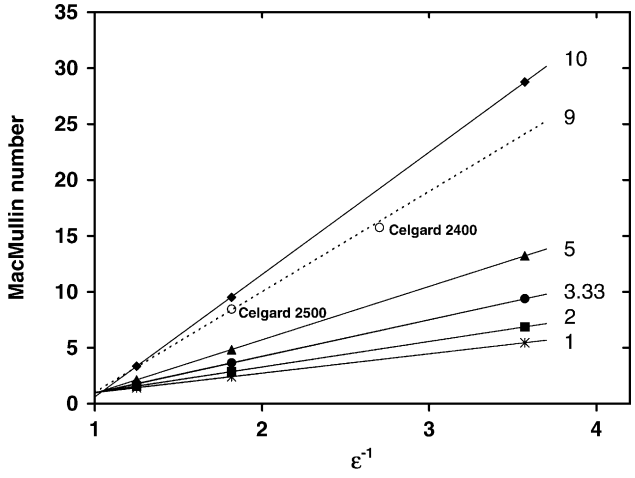

Fig. 9. MacMullin numbers for cubic and rectangular-prismatic particles, dispersed according to Fig. 7, as a function of porosity for various cases of anisotropy, varying from $R = 1$ to $R = 10$. Two separator samples are shown for comparison. Dashed line is calculated from $N_M = 9(1/\varepsilon - 1) + 1$.

$$N_M \cong R\left(\frac{1}{\varepsilon} - 1\right) + 1, \quad \text{for } R \geq 2.5 \tag{12}$$

This provides an interesting relationship between the liquid phase conductivity of a porous body based on its overall porosity and the shape (anisotropy) of its rectangular prismatic particles. It is intriguing to note that two separator products from the same manufacturer, which vary mainly in their porosity values, lie very close to a straight line (calculated for $R = 9$, see Fig. 9). According to results from this work, such a finding would be compatible with a lamellar structure, where the thickness of the lamellae, perpendicular to the separator surface, is almost 10 times smaller than the lengths, parallel to the separator surface.

5. Conclusions

For a liquid phase, simulations confirm the experimental result that a power law (Eq. (3)) is valid for volume fractions from 100% down to about the void volume between closest-packed spheres. The exponent of $\alpha = 1.3$ in the power law is slightly smaller than that reported experimentally for beds of spherical particles ($\alpha = 1.5$) [7,8]. According to numerical simulations presented in this work, arrangements of prolate and oblate ellipsoids also follow a power law, where the Bruggeman exponent increases only slightly to 1.6–1.7 for prolate ellipsoids. For oblate ellipsoids, the Bruggeman exponent increases much more with increasing anisotropy, i.e. the ratio, R, of the main axes. For R-values of 10, Bruggeman exponents of >3 are obtained, and result in significantly lowered effective conductivity through a porous structure which consists of such particles. On the other hand, porous bodies based on cubic particles or platelets do not follow a power law (Eq. (3)) at all. It is found that the MacMullin number increases with increasing anisotropy, i.e. approximately linearly with R and as a linear function of $1/\varepsilon$.

This work corroborates that care has to be taken when liquid phase conductivity of practical battery electrodes is estimated and that a power law (Eq. (1)) with a Bruggeman exponent of 1.5 may severely overestimate ionic conductivity. This investigation shows through relatively simple calculations the clear preference for spherical or slightly prolate ellipsoidal particles for battery electrodes when good high-rate performance is required, since they result in the highest effective electrolytic conductivity through the porous network. Such particles have the additional advantage that the derived electrodes do not pose a risk of being overconsolidated. Even for the case of closest packing, there are still sufficiently wide channels to allow for electrolyte transport. On the other hand, very flat and thin disk or plate-shaped particles should be avoided, at least for high-rate applications, since they drastically reduce electrolytic conductivity.

High formal Bruggeman exponents in the range of typically 3–4 have been derived for a range of separator samples examined in this work and from published data [12]. Such values are an indication of the highly tortuous path inside standard separator materials. It appears that there is room for the development of lower resistance separators, e.g. by developing processes where separator membranes are based on slightly sintered, polymeric or ceramic particles, preferably of spherical shape. Such a morphology could reduce the Bruggeman exponent to around 1.5. Despite a low porosity of $\varepsilon \cong 0.26$, MacMullin numbers of approximately 7.5 could be achieved, which are lower than for most separator products that are available commercially (cf., Table 2). A further advantage of separator products based on relatively tightly packed, quasi-spherical particles could be increased resilience against puncture of the membrane, which thus enables the use of a thinner product and thereby further reduces cell resistance. Some work on separator materials based on ceramic particles has been published recently [13].

No effort has been undertaken in this study to model the morphology of the porous network inside commercially available separators since the effective resistance of a separator layer, saturated with electrolyte solution, can easily be determined experimentally. As pointed out in this work, analogous measurements with free-standing porous electrode layers would be very useful in order to get quantitative information on the electrolyte transport within the electrode pores and to provide better justified morphology parameters for battery design and optimization.

Acknowledgements

The present study was partially supported by a grant from the Foundation for Research, Science & Technology of New Zealand. The authors thank Prof. Michael J. O'Sullivan, University of Auckland, for his continued support of this work and Shu-Yi Chu for performing conductivity measurements.

References

[1] J.S. Newman, C. Tobias, J. Electrochem. Soc. 109 (1962) 1183.
[2] R.E. Meredith, C.W. Tobias, in: C.W. Tobias (Ed.), Advances in Electrochemistry and Electrochemical Engineering, vol. 2, Interscience, New York, USA, 1962, p. 15.
[3] J. Newman, W. Tiedemann, AIChE J. 21 (1972) 25.
[4] T.F. Fuller, M. Doyle, J. Newman, J. Electrochem. Soc. 141 (1994) 1.
[5] M. Doyle, J. Newman, A. Gozdz, C.N. Schmutz, J.-M. Tarascon, J. Electrochem. Soc. 143 (1996) 1890.
[6] R. Spotnitz, in: M. Doyle, E. Takeuchi, K.M. Abraham (Eds.), Rechargeable Lithium Batteries, PV 2000–21, The Electrochemical Society Proceedings Series, Pennington, USA, 2001, p. 457.
[7] R.B. MacMullin, G.A. Muccini, AIChE J. 2 (1956) 393.
[8] R.M. De La Rue, C.W. Tobias, J. Electrochem. Soc. 106 (1959) 827.
[9] M. Doyle, J. Newman, T.F. Fuller, J. Electrochem. Soc. 140 (1993) 1526.
[10] J. Newman, J. Electrochem. Soc. 142 (1995) 97.
[11] D. Fan, R.E. White, J. Electrochem. Soc. 138 (1991) 17.
[12] K.M. Abraham, Electrochim. Acta 238 (1993) 1233.
[13] G. Hörpel, C. Hying, F.-F. Kuppinger, B. Penth, Chem. Ing. Tech. 72 (9) (2000) 973.